Title

Highly Selective Photoelectroreduction of Carbon Dioxide to Ethanol over Graphene/Silicon Carbide Composites

Journal

Angewandte Chemie International Edition, 62(15)

ISSN

1433-7851

Authors

Feng, Guanghui
Wang, Shibin
Li, Shenggang
et al.

Publication Date

2023-04-03

DOI

10.1002/anie.202218664

Highly Selective Photoelectroreduction of Carbon Dioxide to Ethanol over Graphene/Silicon Carbide Composites

Guanghui Feng,[+][a][b] Shibin Wang,[+][a][c] Shenggang Li,[+][a][b][d] Ruipeng Ge,[a][d] Xuefei Feng,[e] Junwei Zhang,[f] Yanfang Song,[a] Xiao Dong,[a] Jiazhou Zhang,[a][d] Gaofeng Zeng,[a][b] Qiang Zhang,[f] Guijun Ma,[d] Yi-De Chuang,[e] Xixiang Zhang,[f] Jinghua Guo,[e] Yuhan Sun,*[a][b][d] Wei Wei,*[a][b][d] and Wei Chen*[a][b]

[a] G. Feng[+], Dr. S. Wang[+], Prof. S. Li[+], R. Ge, Dr. Y. Song, Dr. X. Dong, J. Zhang, Prof. G. Zeng, Prof. Y. Sun, Prof. W. Wei, Prof. W. Chen
Low-Carbon Conversion Science and Engineering Center, Shanghai Advanced Research Institute, Chinese Academy of Sciences, Shanghai 201210, PR China
E-mail: sunyh@sari.ac.cn; weiwei@sari.ac.cn; chenw@sari.ac.cn

[b] G. Feng[+], Prof. S. Li[+], Prof. G. Zeng, Prof. Y. Sun, Prof. W. Wei, Prof. W. Chen
University of Chinese Academy of Sciences, Beijing 100049, PR China

[c] Dr. S. Wang[+]
Institute of Industrial Catalysis, State Key Laboratory Breeding Base of Green-Chemical Synthesis Technology College of Chemical Engineering, Zhejiang University of Technology, Hangzhou 310032, P.R. China

[d] Prof. S. Li[+], R. Ge, J. Zhang, Prof. G. Ma, Prof. Y. Sun, Prof. W. Wei
School of Physical Science and Technology, ShanghaiTech University, Shanghai 201203, PR China

[e] Dr. X. Feng, Dr. Y. Chuang, Prof. J. Guo
Advanced Light Source, Lawrence Berkeley National Laboratory, California 94720, United States

[f] Prof. J. Zhang, Prof. Q. Zhang, Prof. X. Zhang,
Division of Physical Science and Engineering, King Abdullah University of Science and Technology, Thuwal 23955-6900, Saudi Arabia

[+] These authors contributed equally to this work.

Supporting information for this article is given via a link at the end of the document.

Abstract: Using sunlight to produce valuable chemicals and fuels from carbon dioxide (CO_2), i.e., artificial photosynthesis (AP) is a promising strategy to achieve solar energy storage and a negative carbon cycle. However, selective synthesis of C_2 compounds with a high CO_2 conversion rate remains challenging for current AP technologies. We performed CO_2 photoelectroreduction over a graphene/silicon carbide (SiC) catalyst under simulated solar irradiation with ethanol (C2H5OH) selectivity of > 99% and a CO_2 conversion rate of up to 17.1 mmol·gcat−1·h−1 with sustained performance. Experimental and theoretical investigations indicated an optimal interfacial layer to facilitate the transfer of photogenerated electrons from the SiC substrate to the few-layer graphene overlayer, which also favored an efficient CO_2 to C_2H_5OH conversion pathway.

Introduction

Plants absorb large amounts of atmospheric CO_2 to produce food and feedstock via photosynthesis. However, this process has become increasingly overwhelming due to excessive CO_2 emissions from industrial-scale fossil energy consumption, causing a rapid increase in atmospheric CO_2 levels and multifaceted symptoms of global warming.[1] To alleviate this grim situation, the development of efficient artificial photosynthesis (AP), a solar-to-chemical technology,[2] to complement natural photosynthesis is crucial. Although AP has progressed considerably in recent decades,[2,3] efficiently synthesizing valuable chemicals containing carbon–carbon (C–C) bonds and overcoming the usually low CO_2 conversion rates remain challenging.[3c,3d] This is largely owing to the considerable complexity of AP,[2a,3d] which involves multiple sequential and parallel steps, including photoexcitation, charge separation and migration, and redox reactions, to generate the required active intermediates on the catalyst surface. Additionally, thermodynamically favorable C1 products such as carbon monoxide (CO), formic acid (HCOOH), formaldehyde (HCHO), methanol (CH_3OH), and methane (CH_4) can be produced from multiple AP intermediates,[3,4] making it challenging to selectively produce target chemicals containing C–C bonds.[5] Thus, the discovery of catalysts for efficiently synthesizing multicarbon products has been limited, hindering development of advanced AP technology.

The key challenge of the efficient photoconversion of CO_2 to multicarbon compounds is the precise control of active intermediates for C–C coupling while fulfilling the essential photosynthesis steps. We found that this can be achieved using a graphene/silicon carbon (SiC) composite catalyst, which comprises a SiC substrate, interfacial layer (IL), and few-layer graphene overlayer. An optimal IL structure allows photogenerated electrons from the SiC substrate to be facilely transferred to the active sites on the graphene overlayer. Reaction intermediates can then be efficiently formed and stabilized owing to their strong adsorption at the active sites and the high electron density of the graphene surface. Experimental results and first principles calculations show that CH_3OH formation is largely suppressed in favor of C–C coupling. Ethanol (C_2H5OH) is therefore exclusively formed with a selectivity of > 99% and a CO_2 conversion rate of 17.1 mmol·gcat−1·h−1 under simulated solar irradiation with a small bias (−50 mV bias vs. Ag/AgCl) and ambient conditions. Thus, the photoelectrocatalytic performance of our catalyst in producing C_2 products from CO_2 was at least two orders of magnitude higher than those of the state-of-the-art AP catalysts (Table S1).

Results and Discussion

The epitaxial growth of hydrogen-treated commercial hexagonal SiC powder with an average size of 400 nm (denoted as h-S4) at 1500 °C under argon atmosphere (Figure 1a) produced a graphene/SiC composite, denoted as h-GS4. The Raman spectrum of h-GS4 is shown in Figure 1b. The D, G, G*, and 2D peaks at 1350, 1590, 2460, and 2710 cm−1, respectively, indicate the formation of an epitaxial few-layer graphene film,[6] along with the characteristic transvers optical (TO) and longitudinal optical (LO) phonon modes attributed to the SiC substrate.[7] Notably, not all prepared graphene/SiC composites are as efficient as the aforementioned one for CO_2 conversion to C_2H_5OH. For comparison, three additional hydrogen-treated commercial SiC types, namely, 100 nm cubic SiC (c-S1), and 200 nm and 800 nm hexagonal SiC (h-S2 and h-S8, respectively), were used to grow epitaxial few-layer graphene films (see supporting information for details). These few-layer graphene composites were denoted as c-

GS1, h-GS2, and h-GS8, respectively, and their Raman spectra exhibited similar few-layer graphene characteristics and SiC modes (Figure 1b).

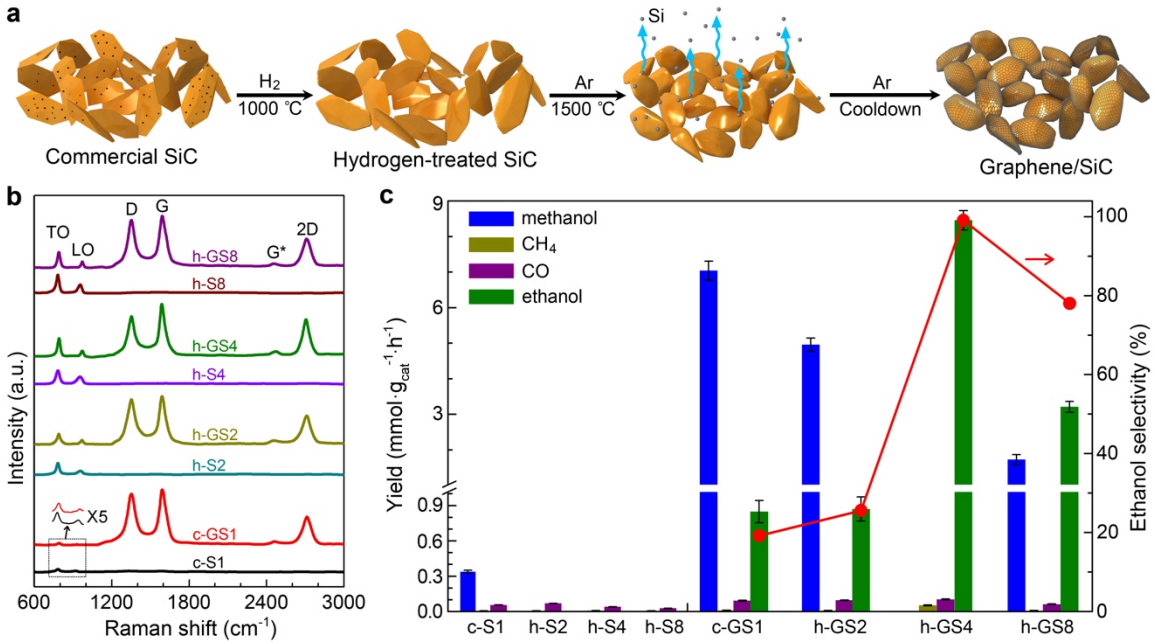

Figure 1. Synthetic scheme, Raman spectra and CO_2 photoelectrocatalytic performances. (a) Schematic of the graphene/SiC composite preparation. (b) Raman spectra of 100 nm cubic SiC (c-S1) and 200 nm (h-S2), 400 nm (h-S4), and 800 nm (h-S8) hexagonal SiC, as well as the corresponding epitaxially grown graphene/SiC composites: c-GS1, h-GS2, h-GS4, and h-GS8. (c) Comparison of the CO_2 photoelectrocatalytic performances of the bare SiC and graphene/SiC samples.

The CO_2 photoelectrocatalytic conversion performances of all the bare SiC and composite graphene/SiC catalysts were compared (Figure 1c), by applying the same reaction conditions of simulated 100 mW·cm−2 AM1.5 solar irradiation and a −50 mV bias (vs. Ag/AgCl) (see supporting information for full details). Only C1 compounds were produced over the bare SiC samples (c-S1, h-S2, h-S4, and h-S8), with CO yields of 20–70 µmol·gcat−1·h−1 and a negligible amount of CH4. The c-S1 sample also produced CH_3OH with a yield of 0.3 mmol·gcat−1·h−1. Overall, the activities of the bare SiC samples were comparable to those previously reported (Table S1).[8] However, interestingly, all the graphene/SiC composite catalysts were capable of converting CO_2 to alcohols, especially C_2H_5OH. The composites c-GS1, h-GS2, and h-GS8 produced both CH_3OH and C_2H_5OH, with small amounts of CO and CH_4. The ethanol selectivity of c-GS1, h- GS2, and h-GS8 were 19%, 26%, and 78%, respectively. In contrast, the only liquid-phase product for h-GS4 was C2H5OH, with high yield of 8.5 mmol·gcat−1·h−1 (Figures S1c and S2a) that was at least two orders of magnitude higher than those of state-of-the-art AP catalysts (Table S1); its yields of CO and CH4 were only 103 and 53 µmol·gcat−1·h−1, respectively, leading to an ethanol selectivity of > 99%. Additionally, the CO_2 conversion rate over h-GS4 was 17.1 mmol·gcat−1·h−1, comparable to those of state-of-the-art catalysts (Table S1),[9] and its solar-to-chemical photo-efficiency was 0.8% (Figure S1e).[6] The reactivities of all composites showed good reproducibility based on > 10 tests each and stable product yields and CO_2 conversion rates over 5 h (Figures S1 and S3), or up to 60 h for h-GS4 (Figures S1e and S3d), with < 5% fluctuation. Post-reaction

scanning electron microscopy (SEM) and transmission electron aberration-corrected microscopy (TEAM) images of h-GS4 after 60 h of testing further showed no distinct alteration in the morphology, structure and catalyst layer thickness (Figure S4). And XRD patterns of h-GS4 also indicated the almost same phase compositions before and after reaction (Figure S5). Isotope-labeling experiments using $13CO_2$ as the reactant confirmed that C_2H_5OH originated solely from the photoelectroreduction of CO_2 (Figure S6). Furthermore, the measured formation rates of molecular oxygen (O_2) from the anodic compartment matched the theoretical values well (Figure S7), implying a stoichiometric reaction between CO_2 and water to produce C_2H_5OH and O_2. The composite h-GS4 distinguished itself from the other catalysts in its exclusive formation of C_2H_5OH, and its specific graphene/SiC interfacial structure appears to be crucial for the efficient C–C coupling.

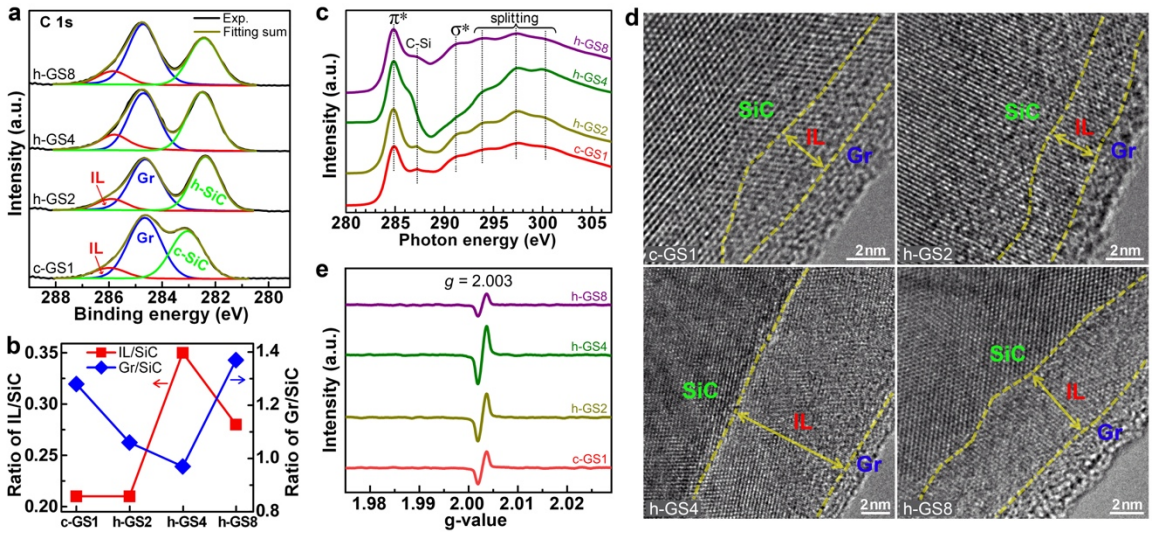

Figure 2. Structural features. (a) XPS spectra of the C 1s level of the composite catalysts. (b) Relative intensity ratios of IL/SiC and Gr/SiC based on the XPS spectra in (a). (c) NEXAFS spectra. (d) High-resolution TEAM images. The yellow dashed lines indicate the lattice boundaries. (e) EPR spectra of the composite catalysts.

The graphene/SiC composite interfacial structures were investigated using X-ray photoelectron spectroscopy (XPS) and near edge X-ray absorption fine structure spectroscopy (NEXAFS). Each XPS C 1s spectra (Figure 2a) was fitted with three components: the substrate cubic SiC (c-SiC) at 283.1 eV or hexagonal SiC (h-SiC) at 282.4 eV, graphene (Gr) layer at 284.7 eV, and IL at 285.9 eV, which are the characteristic peaks for the composites of epitaxial few-layer graphene over SiC.[10] The relative intensity ratios IL/SiC and Gr/SiC for the individual composites are shown in Figure 2b. The IL/SiC ratio was 0.21 for both c-GS1 and h-GS2, indicating that the SiC crystalline phase may not affect the IL configuration. The composite h-GS4 had the largest IL/SiC ratio of 0.35, which was 0.28 for h-GS8. In addition, the Gr/SiC ratios were 1.28, 1.06, 0.97, and 1.37 for c- GS1, h-GS2, h-GS4, and h-GS8, respectively. These results suggest that, among the composites, h-GS4 possesses the highest proportion of IL with the lowest proportion of Gr owing to the deep surface reconstruction induced by the highest intrinsic LO/TO ratio in the h-S4 lattice (Figure S8). The C K-edge NEXAFS spectra of the composites (Figure 2c) were characterized by an intense resonance absorption peak at 284.9 eV and a broadened

peak at 291.2 eV, assigned to the C 1s $\rightarrow \pi^*$ and C 1s $\rightarrow \sigma^*$ transitions,[10c,11] respectively, as well as three split peaks, characteristic of sp2-hybridized carbon atoms,[11] indicating the presence of graphitic structures on the surface. Furthermore, a peak at 287.2 eV was attributed to the subsurface C–Si bonds.[10a,12] In comparison, peak intensities for both the C 1s $\rightarrow \sigma^*$ and C-Si bonds were much lower for h-GS4, suggesting a weak surface in-plane σ^* resonance and unsaturated subsurface C-Si bonds, especially in the IL.

High-resolution TEAM further revealed the configurations of the graphene/SiC composites. As displayed in Figure 2d, all the composites comprised three hierarchical strata, Gr, IL and SiC, with distinct lattice boundaries. Well-defined few-layer graphene was overlaid around the SiC particles (Figures S9 and S10), and the ILs adjacent to the surface were located between the Gr and SiC regions. Furthermore, h-GS4 possessed the thickest IL and thinnest Gr layers (Figure 2d), consistent with the XPS results. Raman analyses (Figure S11) also confirmed that h-GS4 had the thinnest graphene film, as observed by TEAM. Electron paramagnetic resonance (EPR) spectra of graphene/SiC composites showed Lorentz lines of unpaired electrons on π-conjugated carbon atoms (g =2.003), implying the presence of carbon vacancies (Figure 2e).[13] The bare SiC samples had negligible carbon vacancies (Figure S12), and the EPR peak intensities of the graphene/SiC composites were considerably higher than those of their bare SiC counterparts, demonstrating that specific graphene/SiC interface structures derived from the epitaxial growth of SiC substrates have abundant vacancies. Notably, h-GS4 had the highest carbon vacancy concentration, consistent with the NEXAFS results showing the largest unsaturated C–Si bonds in h-GS4.

With a suitable band gap and band edge, SiC can function as an active photoabsorber and catalyze the formation of C1 products from CO_2,[8] whereas the incorporation of a few-layer graphene film and IL boosts C_2H_5OH production and the CO_2 conversion rate. For bare SiC samples, which possess uniform crystalline lattices (Figure S13), the facile recombination of photogenerated electron–hole pairs hinders efficient CO_2 reduction by photoelectrons. The epitaxial growth of few-layer graphene formed interfacial structures in the composites with well-preserved SiC phases (Figure S14), and absorptions in the visible spectrum were enhanced compared with the bare SiC samples (Figure S15). Moreover, the charge transfer resistance (Rct) values of the graphene/SiC composites were smaller than those of the bare SiC samples owing to the conductive few-layer graphene overlayers (Figure S16). The Rct of h-GS4 was only 1.03 Ω, which was ~80% of those of h-GS2 and h-GS8, and 92% of that of c-GS1, implying that electron transfer was the easiest over h-GS4. Thus, the photogenerated electrons from the SiC substrate of h-GS4 could migrate to the graphene overlayer through the IL the most effectively under a bias, affording the largest photocurrent density (Figure S17). The surprisingly high CO_2 conversion rate over h-GS4 could therefore be attributed to the synergistic effects of the best photocurrent response capability and active sites, derived from its intrinsic structural features. Additional experiments demonstrated that the CO_2 photoelectrocatalytic performances of bare SiC and composite graphene/SiC catalysts were not related to their electrochemically active surface areas (Figures S18 and S19) and that a bias of −50 mV enhanced the separation of photogenerated electro–hole pairs, affording substantial product yield improvements for the graphene/SiC composites (Figure S20).

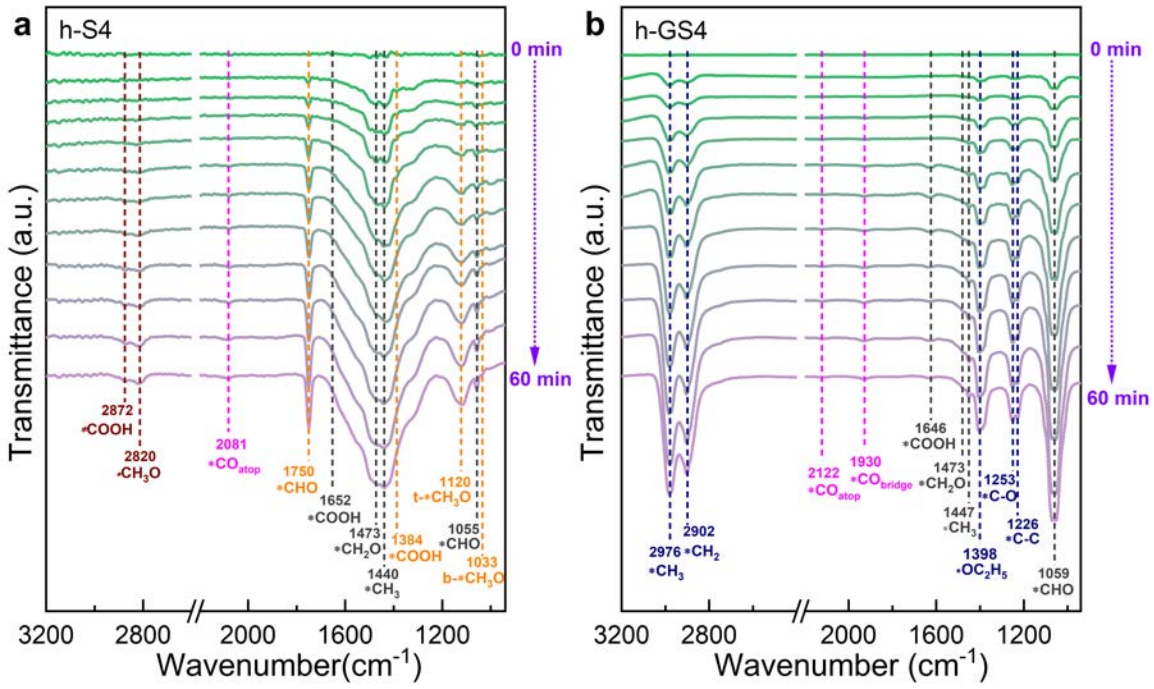

Figure 3. Detection of reaction intermediates. in situ ATR-FTIR spectra of the co-adsorption of a mixture of CO_2 and H_2O vapor over (a) h-S4 and (b) h-GS4 under different light irradiation times.

To obtain the possible reaction pathways and intermediates of CO_2 photoelectrocatalytic conversion over the catalysts, in situ attenuated total reflection Fourier transform infrared (ATR-FTIR) spectra was performed under constant irradiation. A series of peaks appeared over h-GS4 and h-S4 and their intensities were gradually increased in a humid CO_2 atmosphere from 0 to 60 min. As shown in Figure 3a, the peaks over h-S4 at 1384, 1652, and 2872 cm−1 corresponded to C–H bending (δ(C–H)), asymmetric O–C–O stretching, and C–H stretching (ν(C–H)) vibrations of the *COOH group,[14] which is usually considered a key intermediate in CO or CH4 formation. The chemisorbed *CO detected at 2081 cm−1 is essential for forming multielectron products.[15] Furthermore, the signals at 1055 (the H–C=O bending vibration of *CHO), 1473 (*CH_2O), and 1750 cm−1 (C=O stretching vibration of CHO*)[14a,16] represent the crucial intermediates for CH_4 and CH_3OH formation. The band at 2820 cm−1 corresponds to the ν(CH_3) modes of the *H_3CO species, while those at 1120 and 1033 cm−1 correspond to the ν(C–O) modes of bridged (b-OCH3*) and terminal (t-OCH_3*) methoxide species, respectively,[17] indicating the formation of CH_3OH. In-situ ATR-FTIR spectra over h-GS4 (Figure 3b) also showed the similar reaction intermediates at 1646 (corresponding to *COOH), 1473 (*CH2O), and 1059 cm−1 (*CHO), suggesting CO or CH_4 formation. Furthermore, h-GS4 exhibited much higher activity for C_2H_5OH formation with increasing *C_2H_5O characteristic band intensities at 1398 cm−1.[18] The signals at 2902, 1447, and 2976 cm−1 could be attributed to the characteristic symmetric stretching vibrations of *CH_2, and the symmetric and asymmetric stretching vibrations of the *CH3 groups of C_2H_5OH, respectively.[19] The C–OH (1059 cm−1), C–C (1226 cm−1), and C–O (1253 cm−1) groups were also observed as characteristic fingerprint signals of C_2H_5OH.[20] Notably, both h-S4 and h-GS4 clearly showed adsorption peaks at 2081 and 2122 cm−1, respectively, associated with atop-adsorbed *CO (*COatop), while h-GS4 showed an additional adsorption peak at 1930 cm−1 owing to strongly bridge-adsorbed *CO (*CObridge), in

consistent with previous reports.[21] Notably, the blueshift of *COatop over h-GS4 demonstrates strengthened adsorption on the catalyst surface. The carbon vacancies in h-GS4 affect the CO adsorption configuration, leading to more adsorption modes of *CO intermediates compared with bare SiC. (Figure S21)[22] In general, C_2 product formation requires a stronger *CO intermediate that couples with the neighboring *CO.[23] Coexisting *CObridge and *COatop tend to couple to form C_2 products rather than undergo competitive protonation to form *CHO or rapid desorption from the catalyst surface to form CO.[21,24] Consequently, the structural characteristics of h-GS4 enabled the highest carbon vacancy concentration, which facilitated the activation capability of CO_2 and the coupling of key *CO intermediates during CO_2 photoelectroreduction, resulting in the most efficient CO_2 conversion to C_2H_5OH.

To further understand the mechanism of the exclusive formation of C_2H_5OH over h-GS4, we performed extensive density functional theory (DFT) calculations to elucidate the active site structure and the effect of the IL structure on catalytic performance. The photoelectroreduction pathways for CO_2 to C_2H_5OH and CH_3OH were also investigated to understand the structure-selectivity of composite catalysts. CO_2 photoelectrocatalytic reduction includes a set of coupled electron–proton transfer steps, where electron transfer usually occurs at a much shorter time scale than the proton transfer.[25] CO_2 electrocatalytic reduction activity was previously shown to be critically correlated with CO adsorption energy[25] and a moderate CO adsorption energy was further proposed to favor OC–CO dimerization,[26] which is a key elementary step for C_2 product formation from CO_2.[27]

Graphene/SiC composite catalysts were modeled by anchoring a Gr overlayer on the bare Si terminated surface of a SiC substrate (Figure 4a) whose C-terminated surface was passivated by H atoms. The IL was defined as the Si and C atomic layers immediately beneath the Gr overlayer for simplicity (Figure S22). The Gr overlayer of the Gr/SiC model is chemically inert, and CO adsorption energy is merely −0.15 eV (Figure S23) despite the included empirical dispersion correction being a van der Waals interaction, making it an unlikely active site for CO_2 photoelectrocatalytic reduction. Our DFT calculations suggest that creating a C vacancy in the Gr overlayer renders the surrounding unsaturated C sites chemically active, as CO adsorption energies range from −0.5 to −3.6 eV (Figure S23) depending on the relative location of the C vacancy (vac1 and vac2) and CO adsorption configurations (top and bri). In the Grvac1/SiC and Grvac2/SiC models (Figure S22), the three unsaturated C sites in the Gr overlayer directly interacted with two or one Si atoms from the IL with Si–C bond lengths of ~1.85–2.05 Å. In the real catalyst system, the Gr layer that forms heterojunction interfacial layer with the SiC substrate exhibited considerable thickness, as demonstrated in the experimental TEAM result (Figure 2d). However, our calculations on a multi-layered graphene model showed that the Gr layer was stacked via the van der Waals (vdW) interactions, with a calculated layer distance of about 3.9 Å when employing Grimme's empirical vdW dispersion corrections. The optimized structure of the multi-layered graphene model was shown in Figure S24. Since the second/third Gr layer in the model only interact with the SiC substrate via vdW interactions instead of forming the much stronger Si–CGr covalent interactions, the effect of the Gr thickness was considered to be limited on the reactivity in the second/third Gr layer based on our calculations. We thus proposed that only the Gr interfacial layer (IL) that interacted with the SiC matters in determining the reactivity of the h-GS4 catalyst. Furthermore, the main contribution of our present DFT studies using the structure model with only one Gr layer was to propose a plausible

catalytic mechanism for our catalyst and to rationalize the effect of the IL layer and C vacancy sites on the reactivity of CO adsorption and the OC–CO coupling reaction. Bader charge analysis further showed the electron transfer from the relevant Si atoms to C atoms, as the former carries a positive charge of +2.4 |e|, and the latter carries a negative charge of −0.5–−0.7 |e|. Furthermore, several IL structures within the graphene/SiC composite catalysts were modeled by substituting one or three Si atoms in the IL with C atoms (Figures 4a and S22), affording Si:C atomic ratios of 1:1.25 and 1:2 in the IL, respectively.

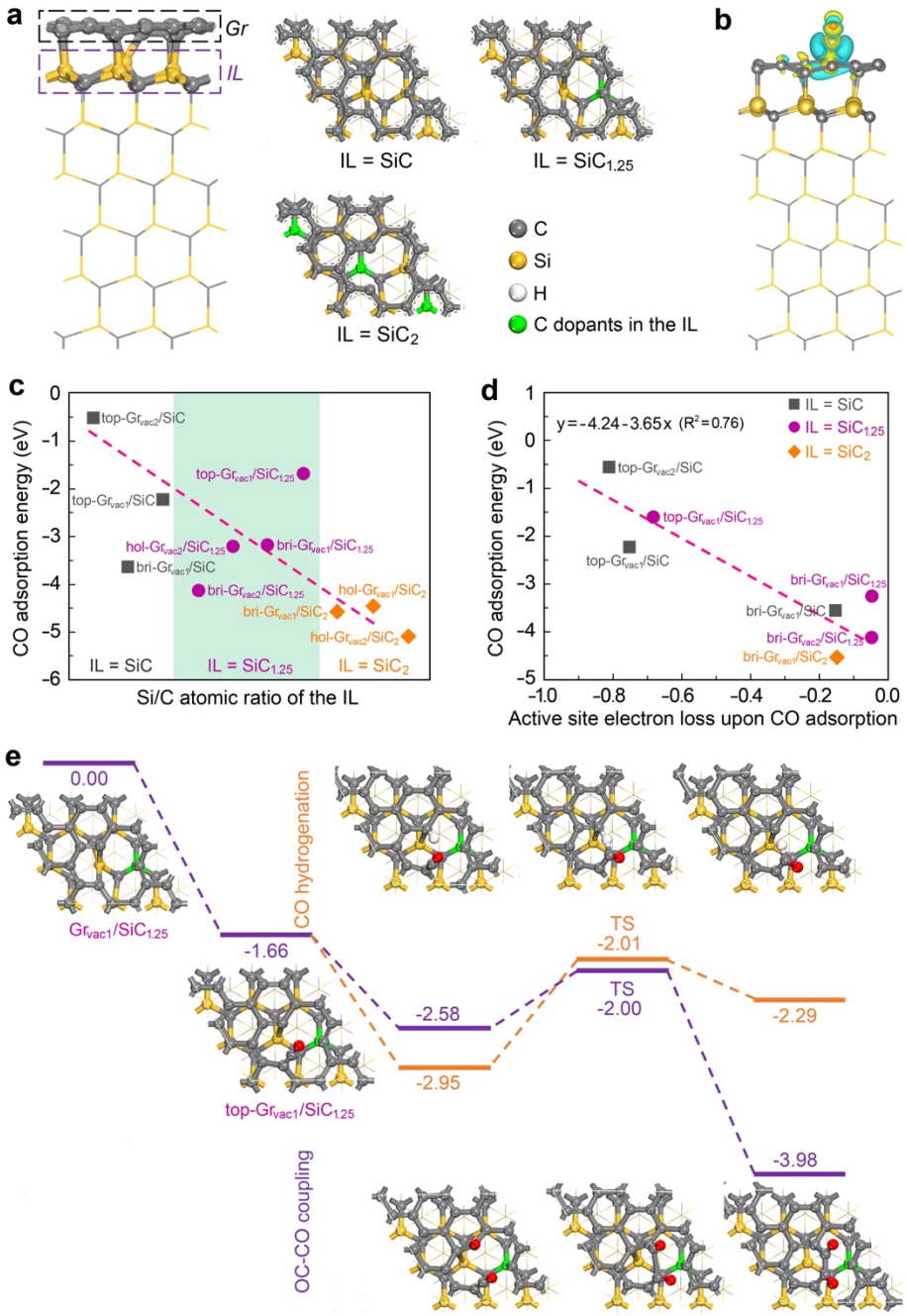

Figure 4. DFT studies. (a) Structural model of a graphene/SiC composite catalyst with the IL and Gr layers over the SiC substrate. (b) Charge density difference plot due to CO adsorption, shown as yellow and cyan isosurfaces for accumulated positive and negative charges, respectively. (c) Calculated CO

adsorption energies versus the Si/C atomic ratios of the IL structure. (d) Calculated CO adsorption energies versus electron loss at the unsaturated C site(s) induced by CO adsorption as predicted by Bader charge analysis. (e) Potential energy surfaces for OC–CO dimerization and CO hydrogenation over the Grvac1/SiC1.25 catalyst model, which favors dimerization over hydrogenation as opposed to that over the Grvac1/SiC catalyst model.

The charge density difference for CO adsorption (Figure 4b) suggests an electron transfer from the graphene layer to CO, consistent with the Bader charge analysis that showed a decrease from 4.53 to 3.78 in the number of valence electrons in the unsaturated C active site upon CO adsorption. The CO adsorbate was predicted to carry a negative charge (−0.23 |e|), indicating an increase in its electron density, while CO adsorption resulted in an unsaturated C active site carrying a positive charge of +0.22 |e| partly owing to the breaking of Si–C bonds. Crystal orbital Hamilton population (COHP) analysis of CO adsorption in the top-Grvac1/SiC structure (Figure S25a) showed that the bond between C in the CO adsorbate and the unsaturated C site in the Gr overlayer arises mostly from their 2s–2p and 2p–2p interactions. In addition, this C@Grvac1–CO bond was predicted to be much stronger than the C@Grvac1–Si@IL bond in the Grvac1/SiC structure, based on calculated integrated COHP (ICOHP) values of −12.64 and −4.11 eV (Figure S23) with corresponding estimated bond energies of 2.19 and 0.20 eV, respectively. The C@Grvac1–CO bond length in the top-Grvac1/SiC structure was very short at 1.33 Å, suggesting a C=C double bond. These results indicate a strong covalent interaction between the CO adsorbate and unsaturated C sites in the Gr overlayer. Furthermore, CO adsorption is generally stronger over catalyst models with higher C concentrations in the IL (Figures 4c and S23), with CO adsorption energies ranging from −1.6 to −4.1 eV for IL = SiC1.25 and −4.4 to −5.1 eV for IL = SiC2. The linear relation between the calculated CO adsorption energy and electron loss at the unsaturated C site upon CO adsorption (Figure 4d) was consistent with the breaking of Si–C bonds and formation of C–C bond during CO adsorption.

Mechanisms for the formation of CH_3OH and C_2H_5OH from CO_2 were further investigated for the Grvac1/SiC and Grvac1/SiC1.25 catalyst models, as shown in Figures S26 and S27, and the calculated reaction energies of the elementary steps were used to tentatively determine possible reaction pathways. Owing to importance of the OC–CO coupling reaction in the formation of C_2 products,[22,27] we calculated its energy barrier and compared with that of CO hydrogenation to reveal the influence of the IL structure on product selectivity. As shown in Figure 4e, after adsorption of the first CO molecule at the top site of one of the three unsaturated C sites in the Gr overlayer in the Grvac1/SiC1.25 model, a second CO molecule can be adsorbed at another unsaturated C site, followed by OC–CO coupling with a low energy barrier of 0.58 eV. In contrast, CO hydrogenation initiated by H adsorption at the other unsaturated C site must overcome a higher energy barrier of 0.94 eV. Therefore, OC–CO coupling is clearly favored over CO hydrogenation, causing the selective formation of C_2 products. In comparison, the Grvac1/SiC model (Figure S28) included OC–CO coupling and CO hydrogenation steps with energy barriers of 0.62 and 0.81 eV, respectively, reflecting only a small difference. Thus, our calculations show OC–CO coupling to be the most important step in C2H5OH formation for the Grvac1/SiC1.25 catalyst model with a higher C concentration in the IL, consistent with the superior performance of h-GS4 with high C concentration in the IL.

Conclusion

We developed a new catalyst comprising graphene and IL over SiC. This catalyst showed a near-perfect C_2H_5OH selectivity of > 99% at an exceedingly high CO_2 conversion rate of 17.1 mmol·gcat−1·h−1 and stability in ambient CO_2 photoelectroreduction. The IL facilitates photogenerated electron transfer from the SiC substrate to the graphene active sites, affording efficient CO_2 activation and C–C coupling to produce C_2H_5OH. This work paves the way toward an advanced AP strategy to efficiently valorize greenhouse CO_2.

Acknowledgements

This work was financially supported by the Ministry of Science and Technology of China (National Key R&D Program of China, 2022YFA1504604), the National Natural Science Foundation of China (nos. 91745114, 21802160), the "Transformational Technologies for Clean Energy and Demonstration", Strategic Priority Research Program of the Chinese Academy of Sciences (no. XDA 21000000), the Hundred Talents Program of Chinese Academy of Sciences (no. 2060299), the Youth Innovation Promotion Association of the Chinese Academy of Sciences (no. E224301401), Shanghai Sailing Program (no. 18YF1425700), Shanghai Pujiang Program (no. 20PJ1415200), the Outstanding Young Talent Project of Shanghai Advanced Research Institute, the Chinese Academy of Sciences (no. E254991ZZ1), the Foundation of Key Laboratory of Low-Carbon Conversion Science & Engineering, Shanghai Advanced Research Institute, Chinese Academy of Sciences (no. KLLCCSE-202207Z, SARI, CAS), Shanghai Functional Platform for Innovation Low Carbon Technology, and the Major Project of the Science and Technology department of Inner Mongolia (no. 2021ZD0020). This work used resources of the Advanced Light Source, which is a DOE Office of Science User Facility under contract no. DE-AC02-05CH11231

Keywords:graphene/silicon carbide • CO_2 photoelectroreduction • ethanol selectivity • promoting C–C coupling

[1] a) C. B. Field, K. J. Mach, Rightsizing carbon dioxide removal. Science 2017, 356, 706-707; b) H. D. Matthews; S. Solomon, Science 2013, 340, 438-439.

[2] a) J. H. Montoya, L. C. Seitz, P. Chakthranont, A. Vojvodic, T. F. Jaramillo, J. K. Nørskov, Nat. Mater. 2017, 16, 70-81; b) C. Liu, B. C. Colón, M. Ziesack, P. A. Silver, D. G. Nocera, Science 2016, 352, 1210-1213; c) A. Listorti, J. Durrant, J. Barber, Nat. Mater. 2009, 8, 929-930.

[3] a) A. Banerjee, G. R. Dick, T. Yoshino, M. W. Kanan, Nature 2016, 531, 215-219; b) K. K. Sakimoto, A. B. Wong, P. Yang, Science 2016, 351, 74-77; c) H. Rao, L. C. Schmidt, J. Bonin, M. Robert, Nature 2017, 548, 74-77; d) W. Tu, Y. Zhou, Z. Zou, Adv. Mater. 2014, 26, 4607-4626.

[4] D. Kim, K. K. Sakimoto, D. Hong, P. Yang, Angew. Chem. Int. Ed. 2015, 54, 3259-3266.

[5] a) C. Han, Y. Lei, B. Wang, Y. Wang, ChemSusChem 2018, 11, 4237-4245; b) H. Li, J. Sun, ACS Appl. Mater. Interace. 2021, 13, 5073-5078; c) W. Weng, S. Wang, W. Xiao, X. W. Lou, Adv. Mater. 2020, 32, 2001560; d) Y. Wang, L. Zhang, X. Zhang, Z. Zhang, Y. Tong, F. Li, J. C.-S. Wu, X. Wang, Appl. Catal. B–Environ. 2017, 206, 158-167.

[6] T. Iwasaki, T. Zelai, S. Ye, Y. Tsuchiya, H. M. Chong, H. Mizuta, Carbon 2017, 111, 67-73.

[7] a) C. Lee, G. Pezzotti, Y. Okui, S. Nishino, Appl. Surf. Sci. 2004, 228, 10-16; b) T. Peng, H. Lv, D. He, M. Pan, S. Mu, Sci. Rep. 2013, 3, 1148.

[8] a) M. A. Gondal, M. A. Ali, M. A. Dastageer, X. Chang, Catal. Lett. 2013, 143, 108-117; b) X. Li, J. Chen, H. Li, J. Li, Y. Xu, Y. Liu, J. Zhou, J. Nat. Gas Chem. 2011, 20, 413-417; c) T. Inoue, A. Fujishima, S. Konishi, K. Honda, Nature 1979, 277, 637-638.

[9] a) W. Zhu, C. Zhang, Q. Li, L. Xiong, R. Chen, X. Wan, Z. Wang, W. Chen, Deng, Z.; Peng, Y., Appl. Catal. B–Environ. 2018, 238, 339-345; b) S. Wang, B. Y. Guan, X. W. D. Lou, Energy Environ. Sci. 2018, 11, 306-310.

[10] a) E. Velez-Fort, A. Ouerghi, M. Silly, M. Eddrief, A. Shukla, F. Sirtti, M. Marangolo, Appl. Phys. Lett. 2014, 104, 093109; b) K.-j. Kim, H. Lee, J. Choi, H. Lee, T. Kang, B. Kim, S. Kim, J. Phys.: Condens. Matter 2008, 20, 225017; c) A. Ouerghi, A. Balan, C. Castelli, M. Picher, R. Belkhou, M. Eddrief, M. Silly, M. Marangolo, A. Shukla, F. Sirotti, Appl. Phys. Lett. 2012, 101, 021603.

[11] a) M. Chowdhury, R. Saito, M. Dresselhaus, Phys. Rev. B 2012, 85, 115410; b) E. Velez-Fort, M. Silly, R. Belkhou, A. Shukla, F. Sirotti, A. Ouerghi, Appl. Phys. Lett. 2013, 103, 083101.

[12] a) C. Kang, L. Fan, S. Chen, Z. Liu, P. Xu, C. Zou, Appl. Phys. Lett. 2012, 100, 251604; b) V. Y. Aristov, G. Urbanik, K. Kummer, D. V. Vyalikh, O. V. Molodtsova, A. B. Preobrajenski, A. A. Zakharov, C. Hess, T. Hänke, B. Büchner, Nano Lett. 2010, 10, 992-995.

[13] a) Q. Wu, Y. Jia, Q. Liu, X. Mao, Q. Guo, X. Yan, J. Zhao, F. Liu, A. Du, X. Yao, Chem 2022, 8, 2715-2733; b) Y. Chen, B. Xi, M. Huang, L. Shi, S. Huang, N. Guo, D. Li, Z. Ju, S. Xiong, Adv. Mater. 2022, 34, 2108621; c) Y. Li, M. Gu, T. Shi, W. Cui, X. Zhang, F. Dong, J. Cheng, J. Fan, K. Lv, Appl. Catal. B–Environ. 2020, 262, 118281.

[14] a) Y. R. Wang, H. M. Ding, X. Y. Ma, M. Liu, Y. L. Yang, Y. Chen, S. L. Li, Y. Q. Lan, Angew. Chem. Int. Ed. 2022, 61, e202114648; b) S. Kattel, B. Yan, Y. Yang, J. G. Chen, P. Liu, J. Am. Chem. Soc. 2016, 138, 12440-12450.

[15] a) J. D. Yi, R. Xie, Z. L. Xie, G. L. Chai, T. F. Liu, R. P. Chen, Y. B. Huang, R. Cao, Angew. Chem. Int. Ed. 2020, 59, 23641-23648; b) X.-F. Qiu, H.-L. Zhu, J.-R. Huang, P.-Q. Liao, X.-M. Chen, J. Am. Chem. Soc. 2021, 143, 7242-7246; c) N. J. Firet, W. A. Smith, ACS Catal. 2017, 7, 606-612.

[16] a) X. F. Qiu, J. R. Huang, C. Yu, Z. H. Zhao, H. L. Zhu, Z. Ke, P. Q. Liao, X. M. Chen, Angew. Chem. Int. Ed. 2022, 134, e202206470; b) X. Yang, J. Cheng, X. Yang, Y. Xu, W. Sun, J. Zhou, Chem. Eng. J. 2022, 431, 134171.

[17] G. L. Chiarello, D. Ferri, E. Selli, Appl. Surf. Sci. 2018, 450, 146-154.

[18] H. Shi, H. Wang, Y. Zhou, J. Li, P. Zhai, X. Li, G. G. Gurzadyan, J. Hou, H. Yang, X. Guo, Angew. Chem. Int. Ed. 2022, 61, e202208904.

[19] A. Fujino, S.-i. Ito, T. Goto, R. Ishibiki, R. Osuga, J. N. Kondo, T. Fujitani, J. Nakamura, H. Hosono, T. Kondo, Phys. Chem. Chem. Phys. 2021, 23, 7724-7734.

[20] a) A. Bielański, A. Lubańska, J. Mol. Catal. A 2004, 224, 179-187; b) Y. Deng, M. Batmunkh, L. Ye, C. Song, T. Ge, Y. Xu, X. Mu, W. Liu, X. Jin, P. K. Wong, Adv. Funct. Mater. 2022, 32, 2110026; c) C. Guo, Y. Guo, Y. Shi, X. Lan, Y. Wang, Y. Yu, B. Zhang, Angew. Chem. Int. Ed. 2022, 134, e202205909.

[21] a) H. Bai, T. Li, S. Cheng, Z. Zhou, H. Yang, J. Li, M. Xie, J. Ye, Y. Ji, Y. Li, Sci. Bull. 2021, 6, 62-68; b) P, Wang, H. Yang, C. Tang, Y. Wu, Y. Zheng, T. Cheng, K. Davey, X. Huang, S. Qiao, Nat. Commun., 2022,13, 3754; c) Z. Tan, M. Haneda, H. Kitagawa, B. Huang, Angew. Chem. Int. Ed. 2022, 61, e202202588; d) S. Zhu, T. Li, W. Cai, M. Shao, ACS Energy Lett., 2019, 4, 682-689.

[22] Y. Zhou, F. Che, M. Liu, C. Zou, Z. Liang, P. De Luna, H. Yuan, J. Li, Z. Wang, H. Xie, Nat. Chem. 2018, 10, 974-980.

[23] W. Wang, C. Deng, S. Xie, Y. Li, W. Zhang, H. Sheng, C. Chen, J. Zhao, J. Am. Chem. Soc. 2021, 143, 2984-2993.

[24] a) T.-C. Chou, C.-C. Chang, H.-L. Yu, W.-Y. Yu, C.-L. Dong, J.-J. s. Velasco-Vélez, C.-H. Chuang, L.-C. Chen, J.-F. Lee, J.-M. Chen, J. Am. Chem. Soc. 2020, 142, 2857-2867; b) M.-P. Jiang, K.-K. Huang, J.-H. Liu, D. Wang, Y. Wang, X. Wang, Z.-D. Li, X.-Y. Wang, Z.-B. Geng, X.-Y. Hou, S. Feng, Chem 2020, 6, 2335-2346; c) Q. Liu, H. Cheng, T. Chen, T. W. B. Lo, Z. Xiang, F. Wang, Energy Environ. Sci. 2022, 15, 225-233; d) R. Das, K. Das, B. Ray, C. P. Vinod, S. C. Peter, Energy Environ. Sci. 2022, 15, 1967-1976.

[25] L. Li, T. Jun Cui, W. Ji, S. Liu, J. Ding, X. Wan, Y. Bo Li, M. Jiang, C.-W. Qiu, S. Zhang, Nat. Commun. 2017, 8, 197.

[26] K. Tran, Z. W. Ulissi, Nat. Catal. 2018, 1, 696-703.

[27] K. Jiang, R. B. Sandberg, A. J. Akey, X. Liu, D. C. Bell, J. K. Nørskov, K. Chan, H. Wang, Nat. Catal. 2018, 1, 111-119.

Table of Contents

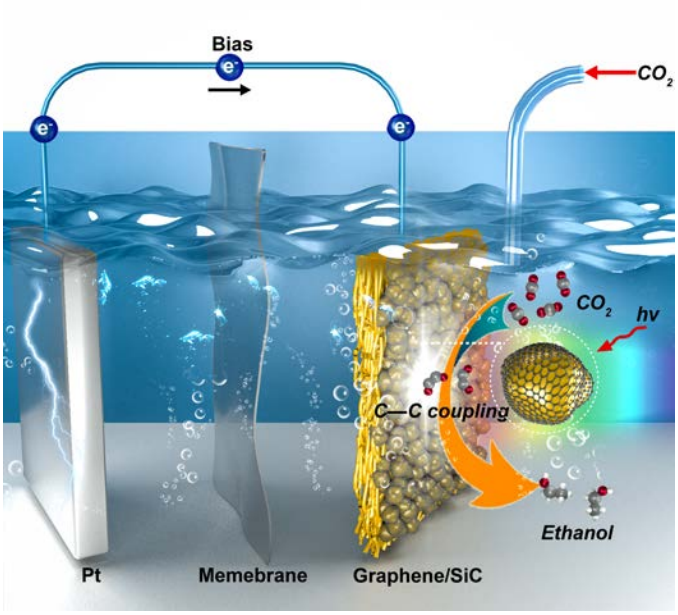

The interfacial layer in the graphene/silicon carbide composite allows the facile transfer of photogenerated electrons from the silicon carbide substrate to the active sites of graphene, resulting in efficient CO_2 activation and C−C coupling for ethanol production. This catalyst showed a near-perfect ethanol selectivity of > 99% at an exceedingly high CO_2 conversion rate of 17.1 mmol·gcat−1·h−1 and stability in ambient CO_2 photoelectroreduction.